Journal Pre-proofs

Structure-function relationships in the feto-placental circulation from in silico interpretation of micro-CT vascular structures

Monika Byrne, Rosalind Aughwane, Joanna L James, Ciaran Hutchinson, Owen Arthurs, Neil Sebire, Sebastien Ourselin, Anna L David, Andrew Melbourne, Alys R Clark

Please cite this article as: M. Byrne, R. Aughwane, J.L. James, C. Hutchinson, O. Arthurs, N. Sebire, S. Ourselin, A.L. David, A. Melbourne, A.R. Clark, Structure-function relationships in the feto-placental circulation from in silico interpretation of micro-CT vascular structures, *Journal of Theoretical Biology* (2021), doi: https://doi.org/10.1016/j.jtbi.2021.110630

- The placenta provides a crucial nutrient exchange surface between mother and fetus
- Delivered placentae exhibit a wide range of vascular branching properties
- Our image-to-model framework aims to relate vascular branching to resistance
- Macro-scale vascular heterogeneities may indicate risk of elevated resistance
- Anastomoses between umbilical arteries mitigate impact of vascular heterogeneity

Title: Structure-function relationships in the feto-placental circulation from in silico interpretation of micro-CT vascular structures

Authors: Monika Byrne[1], Rosalind Aughwane[2], Joanna L James[4], Ciaran Hutchinson[5,6], Owen Arthurs[5,7], Neil Sebire[5,6], Sebastien Ourselin[8], Anna L David[2,3], Andrew Melbourne[8], Alys R Clark[1]

Affiliations:

[1]Auckland Bioengineering Institute, The University of Auckland, Auckland, New Zealand.

[2]Department of Maternal Fetal Medicine, Prenatal Cell and Gene Therapy Group, Elizabeth Garrett Anderson Institute for Women's Health, University College London, London, WC1E 6HX, United Kingdom.

[3]NIHR University College London Hospitals Biomedical Research Centre, 149 Tottenham Court Road, London W1T 7DN, United Kingdom.

[4]Department of Obstetrics and Gynaecology, Faculty of Medical and Health Sciences, University of Auckland, Auckland, New Zealand.

[5]NIHR GOS Institute of Child Health Biomedical Research Centre, University College, London UK

[6]Department of Histopathology, Great Ormand Street Hospital for Children, NHS Trust, London, UK

[7]Paediatric Radiology, Great Ormand Street Hospital for Children, NHS Trust, London, UK

[8]School of Biomedical Engineering and Imaging Sciences, Kings College London, UK

Corresponding Author

A. R. Clark
Auckland Bioengineering Institute
The University of Auckland
Auckland
New Zealand

Email: **alys.clark@auckland.ac.nz**

Abstract

A well-functioning placenta is critical for healthy fetal development, as the placenta brings fetal blood in close contact with nutrient rich maternal blood, enabling exchange of nutrients and waste between mother and fetus. The feto-placental circulation forms a complex branching structure, providing blood to fetal capillaries, which must receive sufficient blood flow to ensure effective exchange, but at a low enough pressure to prevent damage to placental circulatory structures. The branching structure of the feto-placental circulation is known to be altered in complications such as fetal growth restriction, and the presence of regions of vascular dysfunction (such as hypovascularity or thrombosis) are proposed to elevate risk of placental pathology. Here we present a methodology to combine micro-computed tomography and computational model-based analysis of the branching structure of the feto-placental circulation in *ex vivo* placentae from normal term pregnancies. We analyse how vascular structure relates to function in this key organ of pregnancy; demonstrating that there is a 'resilience' to placental vascular structure-function relationships. We find that placentae with variable chorionic vascular structures, both with and without a Hyrtl's anastomosis between the umbilical arteries, and those with multiple regions of poorly vascularised tissue are able to function with a normal vascular resistance. Our models also predict that by progressively introducing local heterogeneity in placental vascular structure, large increases in feto-placental vascular resistances are induced. This suggests that localised heterogeneities in placental structure could potentially provide an indicator of increased risk of placental dysfunction.

Key words

Placenta, haemodynamics, computational model, micro-CT

Introduction

The placenta nourishes the fetus and removes its waste products in pregnancy. To do this efficiently it has a branching tree-like structure that provides a large exchange surface. Impaired placental development and exchange is a major contributor to pregnancy disorders (including fetal growth restriction, FGR), which affects 10-15% of pregnancies and has lasting effects on both mother and fetus[1]. However, our lack of understanding of both normal and impaired placental development means we are unable to predict which pregnancies will be afflicted by these conditions, and to date few effective therapies exist[2]. Those that do show potential, such as low-dose aspirin, need to be administered early in gestation[2], and so early identification of FGR pregnancies is critical.

The outside of each branch of the placental villus tree consists of a bi-layer of specialized placental epithelial cells (trophoblasts) that bathe in maternal blood. The fetal blood vessels are contained within the villi, and are thus physically separated from the maternal circulation. Deoxygenated blood is delivered to the placenta via two umbilical arteries (UAs), which insert at the chorionic plate and spread radially across the placental surface before branching into the large stem villi at the base of the villus trees (Fig. 1a). The vessels continue to branch into progressively smaller vessels, until at the tips of the terminal villi they form capillary loops that are in close proximity to the villus surface, facilitating efficient gas exchange. After passing through the capillaries, oxygenated fetal blood travels back through a network of veins to the umbilical vein (UV), and to the fetus. In most placentae, Hyrtl's anastomosis joins the two UAs. This anastomosis is hypothesized to have an equalizing effect on blood pressure entering regions of the placenta fed by each UA[23]. The absence of this anastomosis may lead to a significant difference in the size of each feeding umbilical artery, a feature which has been associated with a number of morphological abnormalities in the feto-placental vasculature UA[23].
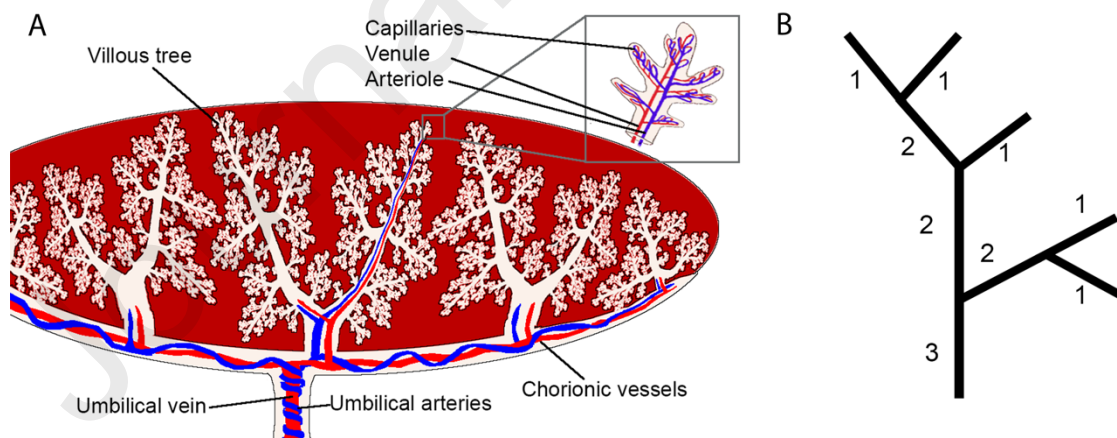

Figure 1: (A) A schematic of the placental vasculature starting from the umbilical cord - two umbilical arteries in blue carrying deoxygenated blood from the fetus and an umbilical vein in red carrying oxygenated blood from the placenta to the fetus. Vessels branch through the chorionic plate and form stem villi which travel towards the basal plate branching into villous trees with arterioles and venules joined by capillary convolutes at terminal villi. (B) A schematic illustrating Shrahler ordering, the method used to quantify placental branching structure. Terminal vessels are labelled order 1 and by moving from terminal vessels to the inlet(s) order is incremented by one each time two vessels of the same order meet.

Effective placental function can be impaired in FGR as a result of structural abnormalities in both the placental and uterine circulations. FGR placentae exhibit reduced villus branching compared with normal placentae, with fewer, longer villi, and impaired vascular branching and density at both the macrovascular (chorionic plate) and microvascular (capillary loop) levels[3,4]. In addition to impairments in blood vessel development, disruption of blood supply in an established placental vascular network can occur due to infarcts (regions of villous tissue necrosis, often due to reduced maternal blood supply), micro-vascular occlusions resulting in avascular or hypovascular terminal villi, or thrombi in the chorionic or stem vessels[5,6]. Whilst such events can occur even in normal pregnancies, these defects are more prevalent in FGR[6]. The consequence of such regional disruptions in the feto-placental circulation is often a significant local reduction in blood flow that could impact whole placental lobes, cotyledons, or much smaller portions of the microvasculature[5]. Furthermore, inadequate adaptation of the uterine circulation by the placenta may impair the volumetric delivery of maternal blood to the placenta, potentially resulting in placental oxidative stress that can inhibit vasodilation in feto-placental vessels. This could contribute to the reduced vessel lumen size observed *ex vivo* in FGR placentae[7].

As the efficiency of the placenta depends on a balance between providing a low resistance vasculature, and maximizing gas exchange, any disruption to the vascular structure could impact these functions. Computational models of the feto-placental circulation have long been used to understand how perturbations to this circulation can impact its function. These models typically simplify the feto-placental vasculature to an averaged (morphometrically derived) representation of structural heterogeneity in the system[8,9]. Although accurate anatomically derived models of components of the system have been developed[10-12], these do not yet extend to the entire feto-placental vasculature. No existing model reflects the variability in the structure of the feto-placental circulation across spatial scales, even in a normal placenta. This means that assessing the impact of pathological features such as vessel constriction, avascular regions or thrombi has been limited.

Micro-focus computed tomography (micro-CT) is emerging as a valuable *ex vivo* tool to assess the feto-placental circulation[13-16]. Computational modelling of the murine feto-placental circulation based on anatomical inputs from micro-CT data has provided significant insights into normal murine vascular function[17,18], and differences in pathological placentation[19]. However, in human studies this integration, while proposed as important[14], has not been implemented. This is in part due to the differences in size and structural complexity of the human placenta compared with the mouse placenta.

Here we present individualised computational descriptions of the human feto-placental vasculature from micro-CT imaging, and use these models to predict the impact of vascular structure on hemodynamic function by linking macro-scale vascular branching with micrometer scale vascular density. Our models predict that local heterogeneity in placental vascular structure can have major impacts on the resistance of the feto-placental circulation and that these heterogeneities potentially provide an indicator of increased risk of placental dysfunction.

Materials and Methods

Micro-CT imaging data

Micro-CT images of the delivered placenta, prepared as described previously[15], were used to construct patient-based models. Placentae were acquired from women undergoing elective term caesarean section following uncomplicated pregnancy at University College Hospital NHS Foundation Trust. Placentae were perfused with Microfil[15], and imaged over their whole volume via micro-CT with isotropic voxel size of 116.5 µm. Perfusion pressure was manually controlled in placental preparation[16], however, comparison of preparation techniques in the human placenta has indicated that vascular filling is comparable in manual versus physiological pressure perfusion[15]. Experimental procedures were approved by Bloomsbury National Research Ethics Service Committee (REC reference number: 14/LO/086, IRAS3133888) and ratified by the University of Auckland Human Ethics Committee.

Two placentae[16], were selected as representations of placentae from normally grown fetuses with 1) a circular appearance with a central cord insertion (P1), and 2) a non-circular appearance with a non-central cord insertion (P2) (Fig. 2).
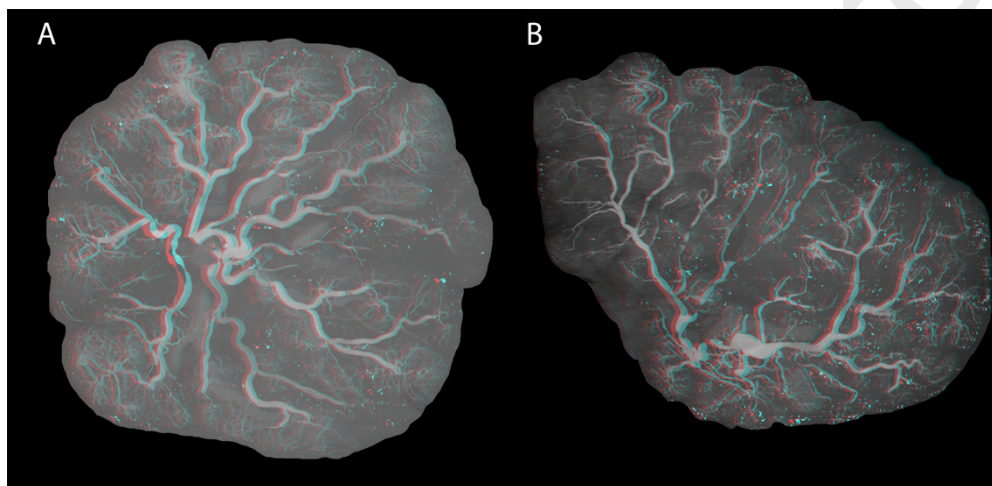

Figure 2: Maximum intensity projections of A) Placenta 1, and B) Placenta 2. Placentae are shown as anaglyphs from which 3D renderings can be visualised.

The macro-vasculature

The imaged voxel size compares to a placental vessel caliber range of 14-4000 µm[20]. Identification of vessel branching from imaging is only accurate for arteries larger than the voxel size. To avoid missing or misidentifying connections between vessels we defined a cut-off vessel size of ≥5 voxels diameter. This allowed definition of explicit branching properties in the chorionic plate, the location of the first vascular branches in the stem villi, and an estimated 2-5 generations beyond the chorionic plate. Beyond this level, vessel trees were generated to reflect vascular density from micro-CT. The methodologies are generalized and with advances in image resolution could be used to define explicit branching structures to any well-defined level of the vasculature.

Segmentation of arterial structures: Arterial structures were segmented using techniques described previously[16]. Whole placenta analysis was performed in MATLAB (R2016b, MathWorks, 2016) using custom-designed algorithms. The axis of the placenta was defined, and a graphical user interface was created allowing the user to open a two-dimensional maximum intensity projection of the whole placenta stack and manually set the point of cord insertion. To define the placental edge, placenta

masks were drawn. MATLAB was used to threshold the placental tissue and vascular tree of each placenta. Manual corrections were applied to restore breaks in the vessel tree and remove areas of Microfil leakage[16].

Conversion of segmented arteries to a graph: A graph of the vascular tree was constructed with elements that represent tree branches and nodes marking branching points (Fig. 3A,B). A MATLAB (version R2018a, Mathworks, 2018) plugin, Skel2Graph3D[21] was modified to account for vessel tortuosity, by creating a new node and element each time the blood vessel changes direction. Custom-written python scripts were used to remove duplicate elements, disconnected nodes, short disconnected branches, and branches that are below the threshold size.
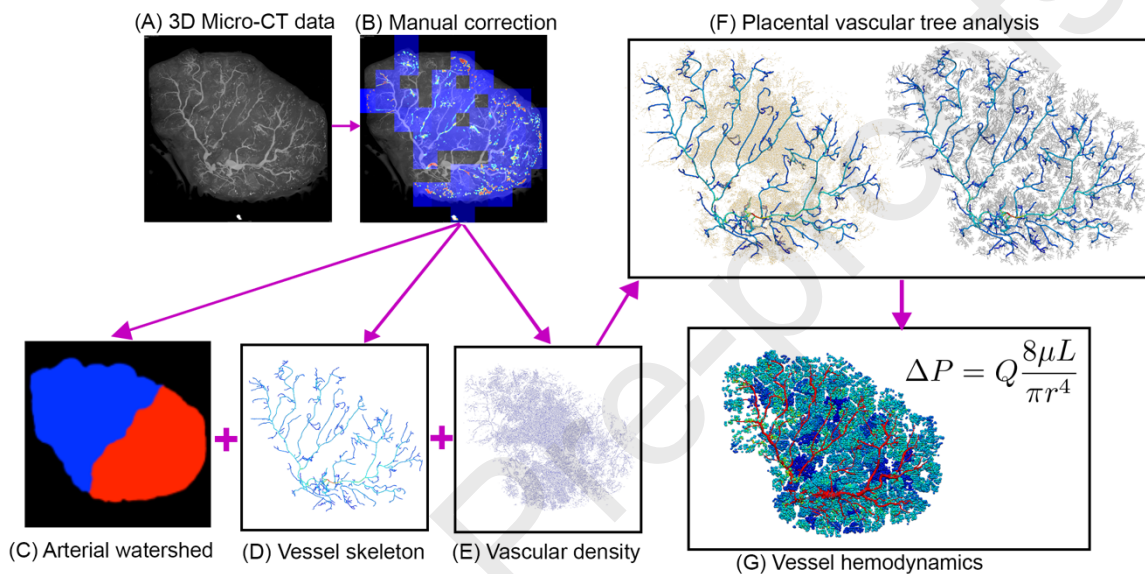

Figure 3: A summary of methods used to generate a placental vascular structure, illustrated for Placenta 2 (with section numbers in which the methodology is described given in the illustration). (A) Micro-CT images are collected[15] and (B) manually corrected[16]. Then, (C) vascular structures are extracted from imaging via thresholding of pixel intensities. (D) Those vessels that can be identified as distinct connected branches are converted to a graphical network structure, defined by segment centreline location in 3D space and vessel radius. (E) Beyond the level of distinct vascular branches, vascular density was defined based on relative brightness of voxels, and (F) a tree structure was generated using the methods of Clark et al.[8]. Finally, (G) blood flow and pressure are simulated in the vessel network using a Poiseuille approximation.

Arterial radius: Radii were determined from the network graph and the surface points of the blood vessel segmentation. A custom-written python script was implemented to: 1) Define a plane perpendicular to the centerline of the vessel. 2) Calculate the distance between the centre-point of the vessel element and each vessel surface point, 3) For each element retain vessel surface points within one voxel of the plane defined in step 1, and not coincident with the center-point. 4) Divide the vessel surface points into 8 equal sectors and eliminate vessel surface points more than two standard deviations from the minimum distance to the center-point sector (dividing the vessel cross-section into sectors allows elliptical cross-sections to be considered). 5) Set the element radius to be the mean of distances between the remaining surface points and the center of the element if the mean is <250% of the shortest distance, or set the radius to the shortest distance. The threshold of 250% was determined by manual assessment of the likelihood of missing an ellipsoidal vessel cross-section against mistakenly including non-physical cross-sections, such as bifurcations.

The meso- and micro-vasculature

Beyond the identified graph, placental blood vessels were generated using a modified volume filling algorithm[8]. This algorithm fills the placental volume with *n* seed points and generates a vascular tree toward those seed points that represents as closely as possible measured morphometric structures in the feto-placental vasculature[8]. The value of *n* approximately represents the number of intermediate villi in the placenta. and *n*=30,000-32,000 produces vascular trees that accurately reflect the number of blood vessels within the placenta and key morphological metrics of feto-placental vascular branching[8]. Local variations in placental vascularity were extracted from micro-CT imaging (Fig. 3C,D). The volume of the placenta was divided into cubes with an edge length of 25voxels. Within these cubes, the total volume of segmented blood vessel (as described previously[16]) not already characterized in the vessel graph was calculated. This provided a 3D map representative of pre-capillary vascular density. Seed points were then generated within each cube by assigning three levels of seed point density (low: 0<vascular density≤0.33, medium: 0.33<vascular density≤0.67, and high: 0.67<vascular density≤1). We then assigned seed point density locally, varying it for low, medium and high regions, to meet the target *n*,[8] and to ensure the effective volume occupied by a seed point reflected the different average densities over each density range. Point separation of 2.00-2.33mm for low, 1.17-1.75mm for medium, and 0.58-1.17mm for high density regions was required to meet these conditions.

Vessel radii for the generated vasculature were calculated based on observed radii for 'average' feto-placental vasculatures in the literature. A Strahler diameter ratio was adjusted to provide trees with terminal villus caliber described in the literature (0.04-0.08mm)[20]. The venous portion was not imaged so was instead generated by copying the geometry of arterial elements (assuming one vein per artery), but the two UAs were replaced by a single UV (as occurs in humans). Venous vessel radii were set to double that of their arterial counterparts[8]. Capillary convolutes were modelled as vessels joining arterioles and venules at terminal villi within a lumped-parameter model accounting for the resistance of the capillaries but maintaining computational tractability[8].

Vascular branching properties

For each tree generated, vascular branching properties were calculated based on the Strahler ordering system (Fig.1b), including the Strahler branching ratio (the factor by which the number of branches decreases in successive Strahler orders, defined across all orders), Strahler length and radius ratios (the rate of decrease in vessel length and radii with Strahler order), and branching angles at each order. As vasculatures with relatively similar major and minor pathways can exhibit different haemodynamic properties to those that have more asymmetry in vessel sizes at bifurcations, we quantified the 'major' (largest) and 'minor' (smallest) branches at each bifurcation[8].

Simulating hemodynamics

Blood flow was simulated as previously described[8]. In brief, the vasculature is represented as a network of cylindrical tubes, and blood flow within them is assumed to be steady state, incompressible, laminar, and with negligible disturbances at bifurcations. This allows Poiseuille approximation for blood flow

$$\Delta P = Q\frac{8\mu L}{\pi r^4}$$

where ΔP is the pressure drop in a vessel, Q is blood flow in the vessel, L is vessel length, μ=3.36x10^{-3}Pa.s is the viscosity of blood, and r is vessel radius. By considering the graph network as an equivalent network of resistors, we sum resistance in series and parallel to determine the total resistance of the system and pressure and flow distributions within it. The micro-vascular model is connected to the macro-vascular model as a single resistive element connecting arteries and veins, with resistance calculated as described by Clark et al.[8]. Pressure continuity and volumetric flow is therefore conserved between the two models.

The inlets to the system are defined as the two UAs that enter the placenta, and the outlet is the UV. At the UV, a fixed pressure is assumed at 20mmHg (2660 Pa)[8]. At the UAs[22], we consider 1) the case of 'normal fetal blood flow' and assume that there is a fixed and equal volumetric flow of blood in each UA, with total UA blood flow of 250ml/min, and 2) the case of 'normal fetal blood pressure' where UA blood pressure is fixed at 50 mmHg[22]. In pathological pregnancies there may be a combination of increased blood pressure and decreased flow due to fetal adaption to pathology, however, assessing these two boundary conditions allows us to predict 1) upper bounds of blood pressure entering the placenta with no fetal adaptation, and 2) upper bounds for the discordance in blood flow through the two umbilical arteries due to asymmetry in placental structures. All calculations used *reprosim* (www.github.com/virtualpregnancy/reprosim).

Results

Properties of generated trees

Analysis of Strahler branching properties in models of placentae P1 and P2 demonstrate asymmetry of vascular branching in both placentae. A complete analysis of branching properties in each tree is provided as supplementary material.

Both P1 and P2 show unequal volumes fed by each UA. In P1 arterial volume is distributed in a 55%:45% ratio, and this ratio is 34%:66% in P2. The diameters of arteries that feed these regions are 3.14mm:3.54mm for P1 and 2.44mm:3.04mm for P2, respectively. P2 is relatively more asymmetric than P1. This asymmetry is also seen in comparing the size of major to minor branches at individual bifurcations. In P2 the level of asymmetry in major to minor branches decreased from the largest chorionic vessels with major branches being 65-79% larger than minor branches in vessels of Strahler order 10-12, reducing to 11-46% over the remainder of the chorionic plate (Strahler order 8-10). P1 had relatively more symmetric chorionic branching with order 8-12 branches showing 0-38% larger major branches than minor.

Fig. 4 shows image-identified regional vascularization in P1 and P2, and the homogenously and heterogeneously generated trees for P2. P2 has higher variability in regional vascularization than P1, there are more and, in places, relatively larger

regions of lower density vasculature. The micro-CT images acquired in P1 showed a total segmented vascular volume of 35.0ml with coefficient of variation (COV) in vascular density of 76.9%. This compares to a total segmented vascular volume of 13.5ml in P2 and a COV in vascular volume of 86.1%. The effect of incorporating a heterogeneous regional vascular density into the generated tree structures does impact on the structure of the vascular tree that is generated, but without consistent changes in the branching statistics.
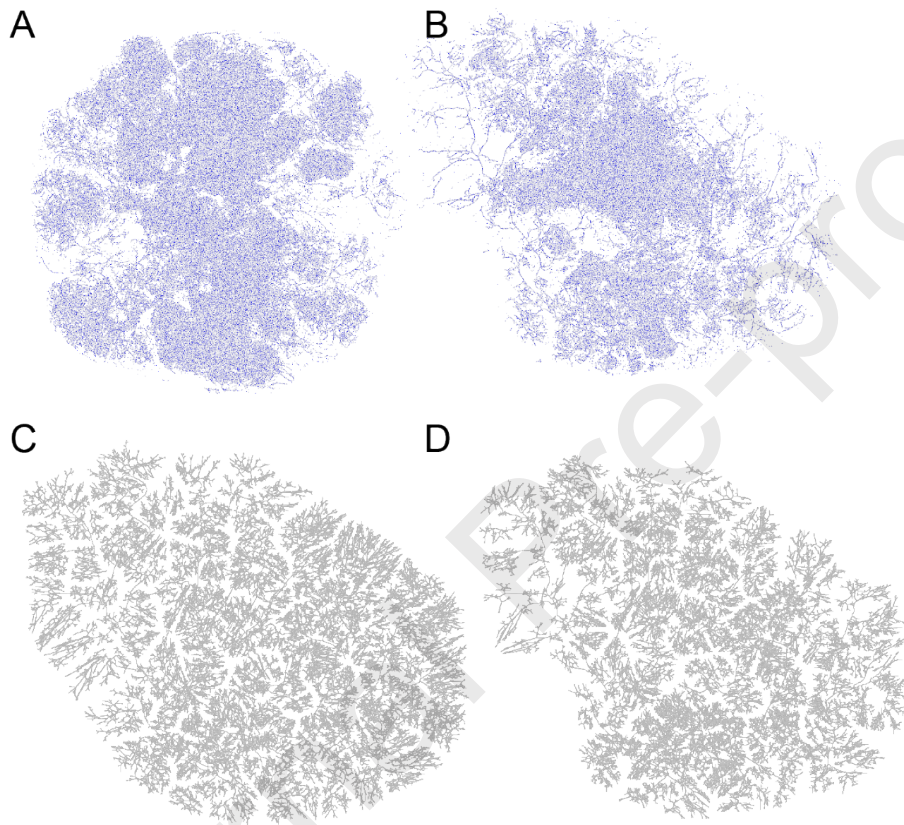

Figure 4: Micro-CT derived maps of vascularity (voxels identified as belonging to arterial centerlines) for (A) Placenta 1 and (B) Placenta 2 highlights that there is more variability in vascular density locally for Placenta 2, although variability exists in both. This results in a distinct regional structure to branching in a generated vascular tree compared with a tree assuming a homogeneous vascular density. (C,D) are generated trees for Placenta 2 with (C) having homogeneous vascular density, and (D) having heterogeneous vascular density.

Hemodynamics

Heterogeneity in vascular structure: To determine the functional impact of differences in vascular symmetry between P1 and P2, blood flow simulations were conducted for each generated vascular tree. Total vascular resistance (the sum in series and parallel of all resistances in the tree) for P1 was 0.73Pa.s/mm^3 and for P2 was 0.86Pa.s/mm^3, which compares to an expected range between 0.64-1.4Pa.s/mm^3 (derived from[31,32], assuming a 30mmHg driving pressure[22]) and reflects a normal vascular resistance, although P2 has a 13.2% higher resistance than P1. Reducing meso-scale vascular

heterogeneity by simulating blood flow in a vasculature generated with uniform vascular density (e.g. Figure 4C), reduces predicted placental resistance in P1 by 5.5% to 0.69Pa.s/mm^3 and in P2 by 2.4% to 0.84Pa.s/mm^3. There is also an increase in variability of placental micro-vascular flow, quantified by COV (standard deviation/mean) in Strahler order 1 vessels, when a heterogeneous vascular density distribution is implemented. With flow boundary conditions applied, for P1 COV=35.7% (homogeneous) and COV=37.9% (heterogeneous), and for P2 COV=55.9% (homogeneous) and COV=59.5% (heterogeneous). Thus, the increased variability in vascular density in P2 results in an increase in flow variability compared to the homogeneous equivalent (Fig. 5). The increased flow heterogeneity in P2 compared to P1 corresponds to the increased COV in vascular density calculated from micro-CT data in P2. Therefore, increased vascular structural heterogeneity is reflected in the model by an increased placental vascular resistance, and increased micro-vascular heterogeneity in flow.
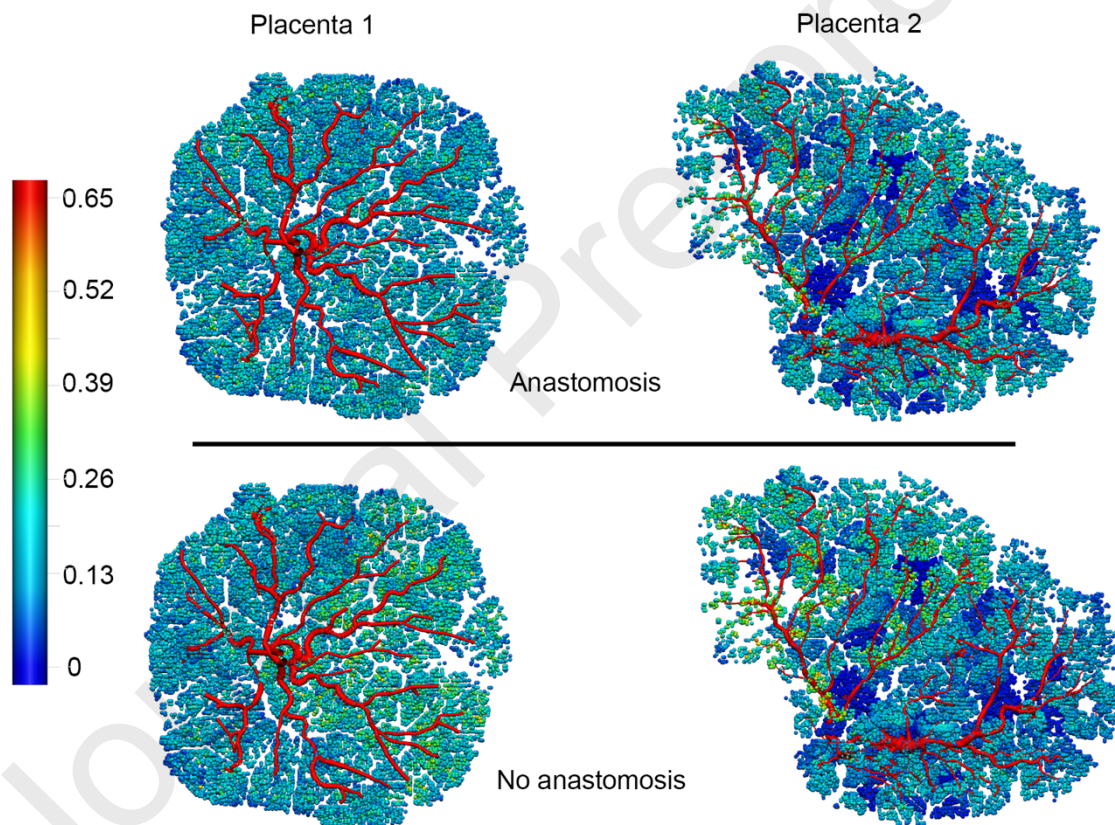

Figure 5: Model predictions for flow distribution in Placenta 1 and Placenta 2 with flow boundary conditions (equal flow in each umbilical artery) with anastomosis and without an anastomosis present between the umbilical arteries. Colour scale shows volumetric flow in mm^3/s.

Hyrtl's anastomosis: While Hyrtl's anastomosis was not visualized with micro-CT, our blood flow simulations were conducted with and without Hyrtl's anastomosis to determine its possible impact. Blood flows and pressures were then assessed at the point of insertion of the UAs into the placental tissue mass). The pressure differential between the two feeding UAs (P_{U1-U2}) was assessed as a metric of asymmetry between the two portions of the placenta. When no anastomosis is included and

250ml/min blood flow is distributed evenly between the two UAs, the model predicts a disproportionate pressure in each UA. In P1, P_{U1-U2}=7.59 mmHg and in P2 P_{U1-U2}=15.34mmHg, reflecting increased asymmetry in P2 compared with P1 P_{U1-U2} increases with flow through the UAs.When an anastomosis is present, this metric is relatively independent of flow delivered, at P_{U1-U2}<0.08mmHg for P1 and P_{U1-U2}<0.15mmHg for P2. So, despite heterogeneity in structure and flow, with an anastomosis, both would function normally. However, with no anastomosis the model predicts a significant impact on the balance of blood pressures between the two UAs in a placenta with heterogenous structure like P2. In addition to changes in driving pressure, a lack of anastomosis is predicted to add 2.42% to COV in order 1 vessel flow over the whole placenta in P1, but in P2 this increases to 6.45%.

With pressure boundary conditions applied, the impact of an anastomosis is to equalize flow upstream of the anastomosis itself, i.e. for blood to be delivered from the fetal circulation equally via each umbilical artery, with an unequal distribution of flow to the portion of the placenta fed by each artery. Even in the relatively symmetric placenta (P1) with pressure boundary conditions applied at the umbilical artery, there is a predicted mis-match in pressure at the entry of the umbilical artery to the chrorionic plate of 1.2mmHg, which compares to a 0.04mmHg difference when Hyrtl's anastomosis is included. Simulations of Hyrtl's anastomosis therefore confirm that the presence of an anastomosis works to equalise pressures between the regions of the placenta fed by each UA.

Perturbations to the feto-placental circulation: While there are several potential causes of a regional reduction in feto-placental blood flow we do not attempt to model driving mechanisms, but instead consider each of these causes as a local restriction to blood flow. We simulate a fixed percentage of vessels of order 1,3,6 and 8 constricted until they receive negligible flow. Order 1 vessels are at the level of intermediate villi, and order 8 vessels feed a region equating approximately to a cotyledon. Thus, we assess both the impact of local restriction of blood flow in the micro-vasculature alone, and across spatial scales to the level of a cotyledon. We occluded randomly distributed vessels over the whole placenta (distributed occlusion), and assessed the effect of one part of the placenta being differentially impacted by simulating the same proportion of vessel occlusion but localizing this to the placental portion fed by a single UA (unilateral occlusion). Random occlusion was defined in the simulation by generating a random number between zero and one, and tagging a vessel as occluded if the random number was less than a defined threshold. Simulations were repeated in the presence or absence of Hyrtl's anastomosis. We assessed these perturbations in the regularly structured P1 placenta only. Images showing the distribution of occluded vasculature in each case (with 40% occlusion) are provided as supplementary material (Figure S1).

The impact of restricting blood flow to order 1 vessels (intermediate villi) is shown in (Figure 6). With an anastomosis between the UAs, UA pressure increases with proportion of the placenta affected. However, the UAs feed the feto-placental circulation at a similar driving pressure. This driving pressure increases with the

percent of arteries occluded, and COV in order 1 blood flow increases. When arterial dysfunction is limited to tissue distal to a single UA, the impact of the same percentage of pathology is reduced when an anastomosis is present: the healthy portion of the placenta is able to accommodate blood flow, mitigating increases in pressure. With no anastomosis, peak umbilical blood pressure (in the impacted artery) is predicted to be significantly elevated and flow heterogeneity is increased. These predictions are consistent when flow or pressure boundary conditions are applied, but the increases in pressure are more significant when flow boundary conditions are applied. These simulations suggest that when small placental blood vessels are occluded a significant increase in placental vascular resistance can be induced, and the presence of Hyrtl's anastomosis can allow a redistribution of blood flow to unaffected regions mitigating the impact of disease when it preferentially impacts the region of the placenta fed by a single UA.
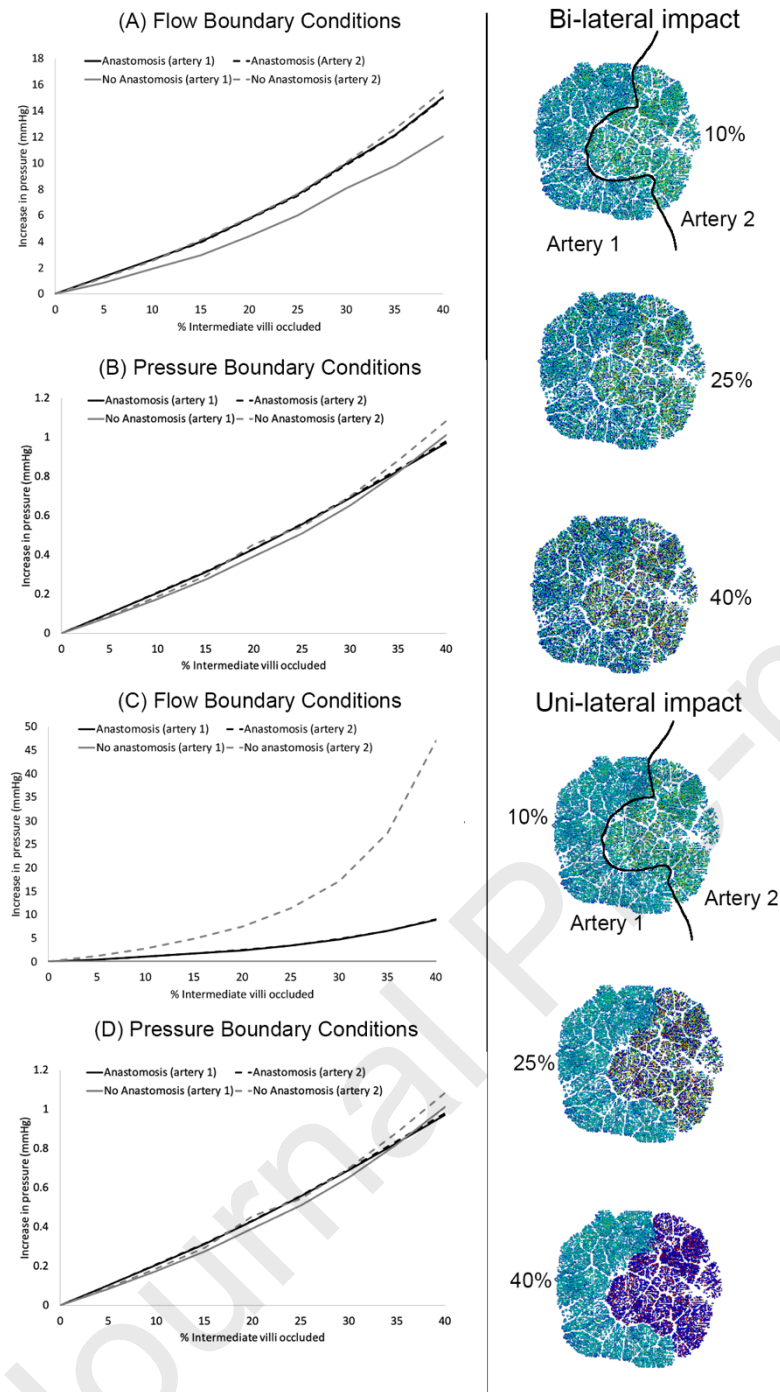
Figure 6: The impact of progressively occluding increasing percentages of order 1 vessels (equivalent to intermediate villi), on blood pressures feeding the placenta in the umbilical arteries. Panels (A,B) show the impact of occlusion in a bilateral manner, and panels (C,D) in a unilateral manner. When an anastomosis is present, the two black lines representing the two umbilical arteries are indistinguishable from one another, however, when the anastomosis is absent there is a pressure differential between the two umbilical arteries and the grey lines representing the two umbilical arteries diverge – this is most pronounced with flow boundary conditions applied to the model (panels A,C) compared with pressure boundary conditions (panels B,D). The right-hand illustrations show diffuse distribution of occluded arteries (bi-lateral impact) in the top three illustrations, and the rbottom three illustrations show the same total percentage occlusion but limited to tissue fed by 'artery 2' (uni-lateral impact). Coloured images in the centre show tissue fed by occluded arteries in dark blue.

The impact of restriction of blood flow to tissue clusters fed by vessels of varying size is shown in Fig. 7. The regions fed by order 8 blood vessels are approximately lobule-sized portions of tissue, and while the model predicts similar trends compared with occlusion of order 1 vessels, the impact of occlusion is more severe across all simulated scenarios. Regardless of the nature of the obliteration (distributed or unilateral), or the presence or absence of an anastomosis, the larger the cluster size (or the higher the order of blood vessel impacted) the greater the impact on predicted UA blood pressure. This is consistent between flow and pressure boundary conditions. With flow boundary conditions applied, the impact of including an anastomosis in the model is to decrease the peak driving pressure (the blood pressure in the highest-pressure artery), and this is most apparent when vascular obliteration is unilateral. When pathology is distributed over the whole placenta the impact of the anastomosis is limited to <4.23mmHg over all the scenarios assessed. With pressure boundary conditions, trends in peak pressure at the point of umbilical artery insertion to the placenta are consistent, but increases in this pressure are smaller than with flow boundary conditions. However, significant reductions in blood flow are predicted when pressure boundary conditions are applied, with up to 45% reduction in total blood flow to the placenta predicted (40% occlusion bilaterally, at order 8).
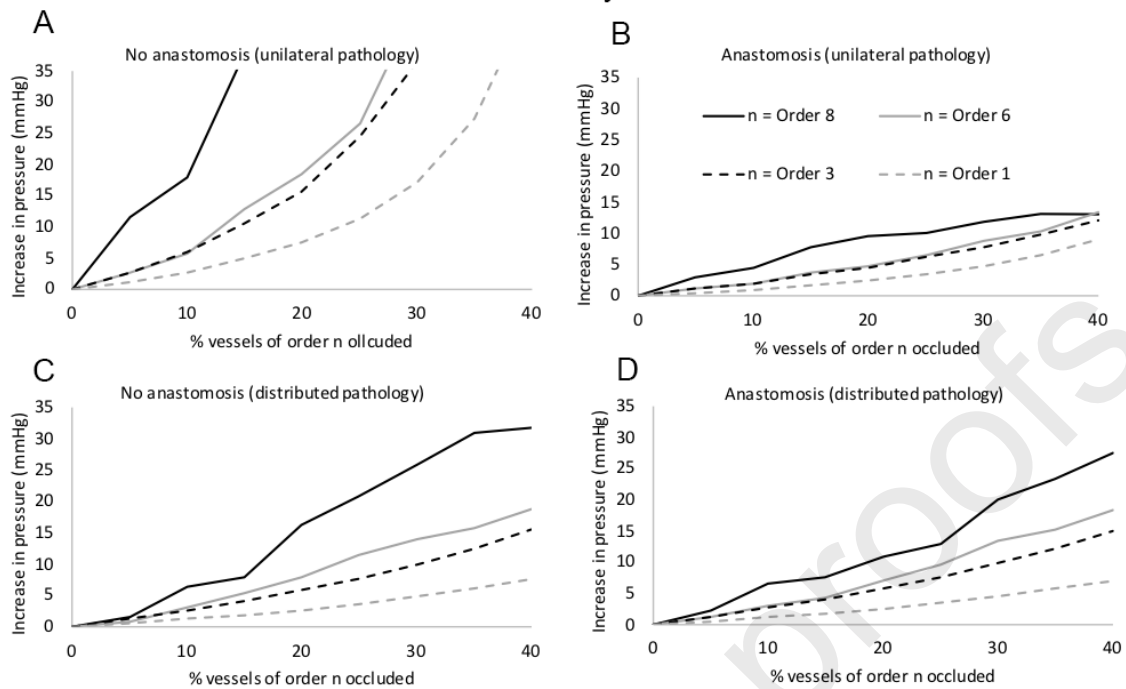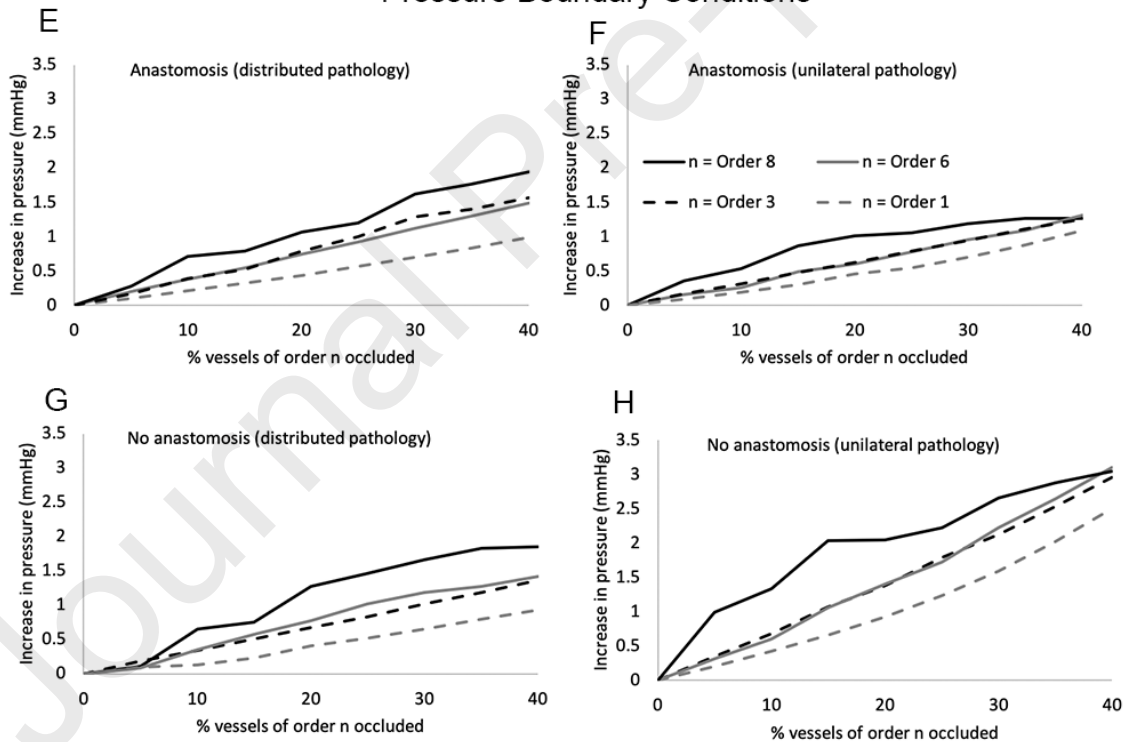
Figure 7: Model predictions of peak umbilical artery blood pressure feeding the placenta for increasing sizes of artery occluded. Results are shown for flow boundary conditions (A-D) and pressure boundary conditions (E-H) The definition of peak umbilical artery pressure is the maximum pressure at the umbilical insertion to the placenta over the two umbilical arteries. Results are shown for (A,E) the case of no anastomosis and unilateral pathology, (B,F) the case of an anastomosis and unilateral pathology, (C,G) no anastomosis with distributed pathology, and (D,H) an anastomosis and distributed pathology. In all cases peak umbilical artery blood pressure is lower when an anastomosis is present than when it is not for the same arterial occlusions.

Discussion

We describe a methodology for generating a computational model of the feto-placental vasculature from whole-placenta micro-CT imaging which allows individualised simulation of how placental structure impacts on its hemodynamic function. By analysing the impact of quantitative measures of feto-placental vascular branching derived from micro-CT on total placental resistance and blood flow heterogeneity, we demonstrate that subject-based anatomy can influence vascular function significantly in normal placentae. Furthermore, we use these models to predict that asymmetry in vascular branching is likely to result in a balance between a low vascular resistance and a large number of small blood vessels available for exchange.

Our model predicted significant impact of placental vascular structure on the heterogeneity of blood flow in the micro-vasculature (at the level of intermediate villi feeding the placental capillary bed). Both example placentae show an increased heterogeneity in micro-vascular blood flow compared to a generic ellipsoidal placenta model with symmetric vascular structure[8]. Regional variability in perfusion in the placenta has been observed using magnetic resonance imaging (MRI) across gestation, with variability within a single placenta and between individuals[33-35]. Zun et al.[33] estimated placental perfusion COV=58±10% in healthy pregnancies. Our predictions of 37.9% and 59.5% in P1 and P2 are consistent with this, noting that predicted perfusion is not directly comparable to MRI and that few proposed MRI protocols separate out maternal and fetal perfusion[36]. We showed that variation in local blood flow heterogeneity does not necessarily lead to higher than normal placental vascular resistance, although there is likely a trend for increasing blood flow heterogeneity to relate to increased vascular resistance. In FGR, structural T2-MRI indicates increased heterogeneity, compared to the relatively homogeneous appearance in normal placentae[34,36]. There are also indications from MRI that placental perfusion heterogeneity is altered in FGR[16,35,37,38]. Although we cannot quantify gas exchange in the model described here, variability in local perfusion may impact matching with oxygenated blood delivery from the maternal circulation and be detrimental to placental exchange function[39].

Increased heterogeneity in blood flow observed in P2 occurs because this placenta has 1) higher variability in local vascular density, 2) smaller caliber (more resistive) chorionic vessels, and 3) some relatively small arteries identified in micro-CT, at the anatomic level of the stem villi. The smaller feeding arteries in some cases correspond to regions of lower vascular density, but this demonstrates that variability in blood vessel caliber near to the chorionic plate (small chorionic arteries and stem villi) can have a significant influence on the flow distribution in the placenta. In this case, the increased number of small vessels at this scale results in a 21.6% increase in COV between P1 and P2, and a 17.8% higher vascular resistance in P2 than P1. Chorionic vascular branching structure has been proposed as an indicator of placental health and efficiency[40]. Our simulations suggest that the size and structure of chorionic vascular arteries may contribute to the overall efficiency of the feto-placental circulation. However, the extent of this role, and whether features of the chorionic

vasculature alone are predictive of dysfunction requires further elucidation in large cohorts of normal and pathological placentae.

We predict that larger clusters of low-perfusion regions (where blood flow redistribution is essentially limited to 'healthy' regions of the placenta) contribute more to elevated placental vascular resistance than smaller, more diffuse regions (in which a more localized redistribution of blood volume can occur, but relatively low resistance pathways through the whole placenta remain). While both placentae we modelled were from normal pregnancies, P2 had a peripheral cord insertion and regions fed by relatively small arteries that our model predicted were less well perfused than others. The impact of the peripheral cord insertion on this placenta was that a relatively small region was fed by one UA rather than the other. Our model predicts that this structure still results in normal function (determined by a normal vascular resistance and normal overall heterogeneity in perfusion). However, it may be that P2 would be more susceptible to insults (should they arise) than P1. The lobular appearance of the placenta on MRI is readily visualised[35-38], but quantifying how this relates to local variability in perfusion and oxygenation is ongoing and challenging to validate. As placental imaging technologies evolve, a combination of MRI imaging, ex-vivo post-delivery assessment, and computational tools such as the model presented here, may shed light on how *in vivo* anatomical and functional heterogeneity relates to physiological and pathophysiological placental features.

Our functional model predicts static resistance, as an indicator of feto-placental vascular function. However, with methodologies for vascular tree extraction and generation in place, a future extension would be to predict the impact of vascular branching structure on dynamic blood flow in the umbilical cord which could be related directly to UA Doppler waveforms[41]. Correlative studies have indicated that an increasing percentage of abnormal feto-placental vasculature increases UA Doppler resistance indices, followed by reversed end-diastolic flow[42]. It has been suggested that the distribution of feto-placental malperfusion may enable risk assessment for fetal compromise[5]. As our model predicts that localized vascular disruption increases feto-placental resistance and flow heterogeneity, it may be expected that this also impacts on Doppler indices.

Hyrtl's anastomosis is observed in the majority of placentae and its absence is associated with discordant UAs, non-central cord insertion, and increased risk of poor outcome[23]. It is hypothesized that the anastomosis plays a role in equalizing blood pressures between the placental lobes fed by each UA[23], and our predictions from our simulations with and without Hyrtl's anastomosis support this. All models with an anastomosis present showed relatively small discordance between blood pressures feeding each lobe (<1 mmHg) compared with larger differences predicted when an anastomosis was not included. The model suggests that this is particularly important when pathology presents asymmetrically (i.e. preferentially in a lobe fed by a single UA). While models exist that predict the impact of Hyrtl's anastomosis on the blood flow and pressure that enters the placenta from the umbilical arteries[22], these models do not incorporate the anatomy of the placental vasculature, and so cannot distinguish

between different presentations of pathology, for example in the case demonstrated here, the difference between clustered and more uniformly distributed pathologies.

We simulated the effect of both flow and pressure boundary conditions applied at the inlet of the umbilical artery (upstream of Hyrtl's anastomosis). These boundary conditions in the context of the umbilical artery and Hyrtl's anastamosis have been described previously[22], and present the extremes of physiologically relevant boundary conditions for this circulation. In both cases, asymmetries in anatomical structure lead to a discordance in pressure at the insertion point of the umbilical arteries into the chorionic plate of the placenta, which is negated when Hyrtl's anastomosis is present (consistent with Gordon et al.[22]). When pathologies were simulated, both pressure and flow boundary conditions showed similar qualitative trends, with greater increases in blood pressure at the cord-insertion to the placenta when larger arteries are occluded. The magnitude of changes in blood pressure at the insertion point is smaller when pressure boundary conditions are applied, however, as driving pressure is fixed across the whole circulation in this case, volumetric blood flow is predicted to reduce considerably (by up to 45% over the cases simulated). The appropriate boundary conditions to apply for placentae with pathology such as FGR likely lie between the two scenarios investigated. While measuring fetal blood pressure in human pregnancies is challenging, animal models of FGR often show an elevated fetal blood pressure[43], there are indications of elevated fetal blood pressure in human FGR pregnancies, leading to cardiac remodelling[44]. Both fetal cardiac output and umbilical venous flow can be significantly reduced in FGR, but there is variability in response with a number of FGR pregnancies exhibiting volumetric flow rates within the normal range[44]. Therefore, there is likely a spectrum of blood pressure and flow adaptions to pathology that lies between the cases simulated in this study – this motivates the use of patient-specific computational flow modelling.

Although the models of the placental vasculature derived in this study are patient-based, they are subject to several limitations. In general, when the whole placenta is imaged with micro-CT the resolution is not sufficient to capture every vascular branch that has been perfused with contrast agent and imaging is subject to the normal considerations of intravascular perfusion techniques[15,36]. However, our graphical representation of arteries derived directly from imaging is reliable to an estimated 2-5 generations beyond the chorionic bed, in images of 116.5μm resolution.

We simulate simplified representations of the fluid dynamics of blood flow within the placenta. These simplifying assumptions have been discussed in detail previously[8,9]. Key assumptions include that of a laminar, fully-developed flow in each blood vessel; a non-compliant vasculature, and that blood can be considered as a Newtonian fluid. Extensions to the model to incorporate a compliant vasculature and non-linear blood rheology are presented as supplementary material. While both assumptions impact on predicted placental vascular resistance, they do not impact the trends presented in this study. Three-dimensional fluid dynamics simulation of flow in the feto-placental vasculature provide a means to investigate the impacts of several of these assumptions, but is typically limited to portions of the placenta[18]. Despite these simplifications our model predicts a vascular resistance and COV in perfusion that is consistent with prior *in vivo* measurements, and this will form a base for future

refinements to geometrical structure and further validation of regional predictions against functional imaging, as these data become available.

In summary, we have shown how models of feto-placental flow can be applied to individual high-resolution placental imaging from micro-CT, and how vascular flow depends on the presence of Hyrtl's anastomoses and adapts to local disruption to the vasculature. We present the methodologies in two real placentae with different shapes and vascular features, and these methods are generalized so that they could be used to predict the function of the feto-placental vascular structure measured from any individual placenta. Future high-resolution imaging and integration of multi-modal *in vivo* information will allow us to model micro-scale vasculature in the feto-placental tree to better understand natural and pathological variability in this fundamental organ.

Conflict of Interest
No benefits in any form have been or will be received from a commercial party related directly or indirectly to the subject of this manuscript.

Acknowledgments

References

1. McCowan LM, Figueras F, Anderson NH. Evidence-based national guidelines for the management of suspected fetal growth restriction: comparison, consensus, and controversy. *Am J Obstet Gynecol.* 2018;218(2):S855-S868.
2. Groom KM, David AL. The role of aspirin, heparin, and other interventions in the prevention and treatment of fetal growth restriction. *Am J Obstet Gynecol.* 2018;218(2):S829-S840.
3. Mayhew T, Ohadike C, Baker P, Crocker I, Mitchell C, Ong S. Stereological investigation of placental morphology in pregnancies complicated by pre-eclampsia with and without intrauterine growth restriction. *Placenta.* 2003;24(2-3):219-226.
4. Krebs C, Macara LM, Leiser R, Bowman AW, Greer IA, Kingdom JCP. Intrauterine growth restriction with absent end-diastolic flow velocity in the umbilical artery is associated with maldevelopment of the placental terminal villous tree. *Am J Obstet Gynecol.* 1996;175(6):1534-1542.
5. Heider A. Fetal vascular malperfusion. *Arch Pathol Lab Med.* 2017;141(11):1484-1489.
6. Salafia CM, Minior VK, Pezzullo JC, Popek EJ, Rosenkrantz TS, Vintzileos AM. Intrauterine growth restriction in infants of less than thirty-two weeks' gestation:

Associated placental pathologic features. *Am J Obstet Gynecol.* 1995;173(4):1049-1057.

7. Burton GJ, Jauniaux E. Pathophysiology of placental-derived fetal growth restriction. *Am J Obstet Gynecol.* 2018;218(2):S745-S761.

8. Clark A, Lin M, Tawhai M, Saghian R, James J. Multiscale modelling of the feto–placental vasculature. *Interface focus.* 2015;5(2):20140078.

9. Tun WM, Yap CH, Saw SN, James JL, Clark AR. Differences in placental capillary shear stress in fetal growth restriction may affect endothelial cell function and vascular network formation. *Sci Rep.* 2019;9(1):9876.

10. Pearce P, Brownbill P, Janáček J, et al. Image-based modeling of blood flow and oxygen transfer in feto-placental capillaries. *PloS one.* 2016;11(10):e0165369.

11. Plitman Mayo R, Charnock-Jones DS, Donoghue K, Oyen ML, Burton G. Three-dimensional modeling of human placental terminal villi. *Placenta.* 2016;43:54-69.

12. Erlich A, Pearce P, Mayo RP, Jensen OE, Chernyavsky IL. Physical and geometric determinants of transport in fetoplacental microvascular networks. *Science advances.* 2019;5(4):eaav6326.

13. Langheinrich AC, Vorman S, Seidenstücker J, et al. Quantitative 3D micro-CT imaging of the human feto-placental vasculature in intrauterine growth restriction. *Placenta.* 2008;29(11):937-941.

14. Junaid TO, Bradley RS, Lewis RM, Aplin JD, Johnstone ED. Whole organ vascular casting and microCT examination of the human placental vascular tree reveals novel alterations associated with pregnancy disease. *Sci Rep* 2017;7(1):4144-4144.

15. Pratt R, Hutchinson JC, Melbourne A, et al. Imaging the human placental microcirculation with micro-focus computed tomography: Optimisation of tissue preparation and image acquisition. *Placenta.* 2017;60:36-39.

16. Aughwane R, Schaaf C, Hutchinson JC, et al. Micro-CT and histological investigation of the spatial pattern of feto-placental vascular density. *Placenta.* 2019;88:36-43.

17. Rennie MY, Cahill LS, Adamson SL, Sled JG. Arterio-venous fetoplacental vascular geometry and hemodynamics in the mouse placenta. *Placenta.* 2017;58:46-51.

18. Bappoo N, Kelsey LJ, Parker L, et al. Viscosity and haemodynamics in a late gestation rat feto-placental arterial network. *Biomech Model Mechan.* 2017;16(4):1361-1372.

19. Rennie MY, Detmar J, Whiteley KJ, et al. Vessel tortuousity and reduced vascularization in the fetoplacental arterial tree after maternal exposure to polycyclic aromatic hydrocarbons. *Am J Physiol Heart Circ.* 2010;300(2):H675-H684.

20. Leiser R, Kosanke G, Kaufmann P. Human placental vascularization. In: *Placenta: basic research for clinical application.* Karger Publishers; 1991:32-45.

21. Kollmannsberger P, Kerschnitzki M, Repp F, Wagermaier W, Weinkamer R, Fratzl P. The small world of osteocytes: connectomics of the lacuno-canalicular network in bone. *New J Physics.* 2017;19(7):073019.

22. Gordon Z, Eytan O, Jaffa AJ, Elad D. Hemodynamic analysis of Hyrtl anastomosis in human placenta. *Am J Physiol Reg I.* 2007;292(2):R977-R982.

23. Raio L, Ghezzi F, Di Naro E, Franchi M, Brühwiler H. Prenatal assessment of the Hyrtl anastomosis and evaluation of its function: case report. *Hum Reprod.* 1999;14(7):1890-1893.

24. Boyd PA. Quantitative structure of the normal human placenta from 10 weeks of gestation to term. *Early human development.* 1984;9(4):297-307.

25. de Paula CFS, Ruano R, Campos JADB, Zugaib M. Placental Volumes Measured by 3-Dimensional Ultrasonography in Normal Pregnancies From 12 to 40 Weeks' Gestation. *Journal of Ultrasound in Medicine.* 2008;27(11):1583-1590.

26. Haeussner E, Schmitz C, von Koch F, Frank HG. Birth weight correlates with size but not shape of the normal human placenta. *Placenta.* 2013;34(7):574-582.

27. Benirschke K, Kaufmann P, Baergen R. Pathology of the human placenta. 2000. In: New York: Springer.

28. Kosanke G, Castellucci M, Kaufmann P, Mironov VA. Branching patterns of human placental villous trees: Perspectives of topological analysis. *Placenta.* 1993;14(5):591-604.

29. Haeussner E, Buehlmeyer A, Schmitz C, Von Koch FE, Frank H-G. Novel 3D microscopic analysis of human placental villous trees reveals unexpected significance of branching angles. *Scientific reports.* 2014;4:6192.

30. R.Leiser GKPK. Human Placental Vascularization: Structural and Quantative Aspects. *Soma H(ed): Placenta: Basic Research for Clinical Application Int Conf on Placenta, Tokyo, 1990, Basel, Karger, 1991, pp 32-45.* 1990.

31. Kiserud T, Rasmussen S, Skulstad S. Blood flow and the degree of shunting through the ductus venosus in the human fetus. *Am J Obstet Gynecol.* 2000;182(1):147-153.

32. Kiserud T, Ebbing C, Kessler J, Rasmussen S. Fetal cardiac output, distribution to the placenta and impact of placental compromise. *Ultrasound Obstet Gyn.* 2006;28(2):126-136.

33. Zun Z, Zaharchuk G, Andescavage NN, Donofrio MT, Limperopoulos C. Non-Invasive Placental Perfusion Imaging in Pregnancies Complicated by Fetal Heart Disease Using Velocity-Selective Arterial Spin Labeled MRI. *Sci Rep.* 2017;7(1):16126.

34. Damodaram M, Story L, Eixarch E, et al. Placental MRI in intrauterine fetal growth restriction. *Placenta.* 2010;31(6):491-498.

35. Sinding M, Peters DA, Poulsen SS, et al. Placental baseline conditions modulate the hyperoxic BOLD-MRI response. *Placenta.* 2018;61:17-23.

36. Aughwane R, Ingram E, Johnstone ED, Salomon LJ, David AL, Melbourne A. Placental MRI and its application to fetal intervention. *Prenat Diagn.* 2020;40(1):38-48.

37. Ingram E, Morris D, Naish J, Myers J, Johnstone E. MR imaging measurements of altered placental oxygenation in pregnancies complicated by fetal growth restriction. *Radiology.* 2017;285(3):953-960.

38. Sinding M, Peters DA, Frøkjaer JB, et al. Placental T2* measurements in normal pregnancies and in pregnancies complicated by fetal growth restriction. *Ultrasound Obstet Gyn.* 2015.

39. James JL, Chamley LW, Clark AR. Feeding your baby in utero: how the uteroplacental circulation impacts pregnancy. *Physiology.* 2017;32(3):234-245.

40. Shah R, Girardi T, Ma X, Salafia C. Fractal dimensions and branching characteristics of placental chorionic surface arteries. *Placenta.* 2018;70:4-6.

41. Thompson RS, Trudinger BJ. Doppler waveform pulsatility index and resistance, pressure and flow in the umbilical placental circulation: an investigation using a mathematical model. *Ultrasound Med Biol.* 1990;16(5):449-458.

42. Morrow RJ, Adamson SL, Bull SB, Ritchie JK. Effect of placental embolization on the umbilical arterial velocity waveform in fetal sheep. *Am J Obstet Gynecol.* 1989;161(4):1055-1060.

43. Morrison JL. Sheep models of intrauterine growth restriction: fetal adaptations and consequences. *Clin Exp Pharmacol Physiol.* 2008;35(7):730-743.
44. Kiserud T, Ebbing C, Kessler J, Rasmussen S. Fetal cardiac output, distribution to the placenta and impact of placental compromise. *Ultrasound Obstet Gynecol.* 2006;28(2):126-136.

-

Monika Byrne: Conceptualization, Methodology, Software, Writing - Original Draft, Writing - Review & Editing.

Rosalind Aughwane: Methodology, Investigation, Data Curation, Writing - Review & Editing.

Joanna L James: Conceptualization, Methodology, Writing – Original Draft, Writing - Review & Editing, Supervision.

Ciaran Hutchinson: Resources, Conceptualization, Writing - Review & Editing.

Owen Arthurs: Resources, Conceptualization, Writing - Review & Editing.

Neil Sebire: Resources, Conceptualization, Writing - Review & Editing.

Sebastien Ourselin: Conceptualization, Supervision, Funding Acquisition, Writing - Review & Editing.

Anna L David: Conceptualization, Supervision, Writing - Review & Editing.

Andrew Melbourne: Conceptualization, Methodology, Software, Writing - Original Draft, Writing - Review & Editing, Supervision.

Alys R Clark Conceptualization, Methodology, Software, Writing - Original Draft, Writing - Review & Editing, Supervision

-